Bioorthogonal tools to study fatty acid uptake in immune cells

Bertheussen, K.

2

Live-Cell Imaging of Sterculic Acid by Bioorthogonal Reaction with Tetrazine-Fluorophore Conjugates

Abstract

In the field of lipid research, bioorthogonal chemistry has made the study of lipid uptake and processing in living systems possible, whilst minimising artefacts on their biology resulting from pendant detectable groups. To allow the study of unsaturated free fatty acids in live cells, this Chapter reports the first use of sterculic acid, a naturally occurring 1,2-cyclopropene-containing fatty acid, as a bioorthogonal probe that can be reacted in the live-cell compatible Inverse Electron-Demand Diels-Alder Reaction (IEDDA). The fatty acid can be readily taken up by dendritic cells without toxic side-effects, and it can subsequently be visualised using a IEDDA reaction with quenched tetrazine-fluorophore conjugates. This reaction can also be integrated into a multiplexed bioorthogonal reaction workflow by combining it with two sequential copper-catalysed azide-alkyne cycloaddition reactions. This allows for the simultaneous study of uptake and incorporation of multiple biomolecules in the cell by multimodal confocal imaging.

This chapter is adapted from the publication:

K. Bertheussen, M. van de Plassche, T. Bakkum, B. Gagestein, I. Ttofi, A. J. C. Sarris, H. S. Overkleeft, M. van der Stelt, S. I. van Kasteren, *Angew. Chem. Int. Ed.* **2022**, *61*.

Introduction

Lipids serve a myriad of roles in biology; as a catabolic carbon source[1], components of cellular and organellar membranes[2], post-translational protein modifications[3], and signalling molecules[4]. The study of their contributions in biology is complicated by their lack of direct genetic encoding, their inherent lipophilicity, and the fact that chemical modifications, e.g. with pendant fluorophores, can severely alter their structure and biochemical properties.[5]

As a result, major efforts have gone into applying bioorthogonal chemistry to the study of lipid biochemistry. By introducing small terminal alkynes and azides in fatty acid tails[6–11], phospholipids[12,13], sphingolipids[14], and cholesterol[15–17], it has been possible to study lipids with only minimal modifications compared to the endogenous molecules. This strategy reduces the chances of the modifications affecting the native function of the lipid and has successfully been used to study lipid localisation[10,12,13,17], metabolism[11,16], and trafficking[18–20], as well as post-translational lipidation of proteins (reviewed by Distefano and co-workers[21]). However, the downside of labelling lipids with alkynes/azides has been the lack of live-cell compatible chemistries that can be used with low background reactivity and fast reaction rates.[22,23] Another complicating factor when performing bioorthogonal ligation on lipids is imposed by the hydrophobic environment in which the probes reside. Optimising the fluorescent reaction partners, particularly for live-cell imaging, is thus necessary.

In 2008, the groups of Fox and Weissleder reported the inverse electron demand Diels-Alder (IEDDA) reaction – the reaction between an electron-poor diene, such as a tetrazine, and a strained or electron-rich dienophile – as a new bioorthogonal reaction.[24,25] This reaction was considered highly favourable for live-cell use due to its high reaction rates and the fluorescence quenching properties of the tetrazine (reviewed by Bernardes and co-workers[26]). The most used dienophile, *trans*-cyclooctene (TCO), is a relatively large modification compared to terminal alkynes or azides[27], but has been used successfully to label, among others, the Golgi-membrane with a TCO-modified ceramide probe.[28,29] However, for most lipids where chemical modifications to the structure can largely affect their function, smaller dienophiles are needed.[5,19] An important advance in the application of the IEDDA reaction to live-cell studies of lipid function, was the development of sterically minimal dienophiles. To this end allyl-thiols were reported by Bernardes and co-workers.[30] However, these proved to have rather slow reaction kinetics (≤ 0.002 $M^{-1}s^{-1}$). Devaraj and co-workers[31], and Prescher and co-workers[32] simultaneously reported cyclopropenes, so-called MiniTags, as minimal reactive dienophiles[33,34]. These cyclopropenes were incorporated into the head groups of phospholipids and were capable of reacting with rate constants of up to 13 $M^{-1}s^{-1}$ in an IEDDA reaction[31], whilst only being slightly larger than alkynes and azides[27]. However, since the modifications were made in the phospholipid head groups, they could not be used to study fatty acid biology and the modification of proteins with fatty acids. Still, the above-mentioned properties make them an attractive alternative to TCO. Cyclopropenes are also reported to have been incorporated into glycans[32,35], lignin polymers[36], and nucleotides[37], combined with live-cell IEDDA reaction and imaging, emphasising their applicability as a bioorthogonal probe.

As discussed by Row and Prescher, it is often useful to look to nature for new bioorthogonal probes, as even rare motifs present in natural products indicate stability and compatibility in living systems.[27] In light of this, Nunn's 1952 discovery[38] of the plant metabolite sterculic acid (StA), a carbocyclic fatty acid[39] found in the kernels of *Sterculia foetida*, was intriguing. This 18-carbon *cis*-unsaturated lipid contains a naturally occurring 1,2-substituted cyclopropene-ring at C9-C10. In plants, it is synthesised by addition of a methylene unit to the double bond of oleic acid (18:1, *cis*-9), followed by enzymatic dehydrogenation to yield the cyclopropene ring.[40] It was not known whether this molecule could be used in live-cell compatible labelling chemistry as a bioorthogonal oleic acid analogue, but it is known to be biologically stable and represents a minimal structural modification of one methylene group compared to the parent oleic acid structure. Furthermore, all previously described bioorthogonal IEDDA applications have been explored for cyclopropenes with 1,3-, 3,3- or 1,2,3-substitution patterns[31,32,41], whereas there has been no report of a 1,2-substituted cyclopropene as a bioorthogonal probe.

Here, the use of StA as a bioorthogonal probe was assessed for its reaction kinetics, short-term toxicity, and live- and fixed-cell imaging capability. It was shown that the fatty acid was readily taken up by dendritic cell lines and could be used for live-cell microscopy by reaction with a tetrazine-fluorophore conjugate (Figure 1). The reaction was furthermore explored in a multiplexed reaction setup.[42] Multiple groups have previously described that it is possible to combine up to three bioorthogonal ligation reactions in a triple mutually orthogonal system, which allows the tracking of multiple bioorthogonally labelled biomolecules in a single sample.[43–45] Previous efforts in the group have focussed on the multiplexing of two copper-catalysed azide-alkyne cycloaddition (CuAAC) reactions.[46] Here, it was explored whether StA also proved compatible with the CuAAC reactions, allowing a triple-click labelling strategy. These experiments all indicate that StA is a valuable reagent to study fatty acid uptake in immune cells.

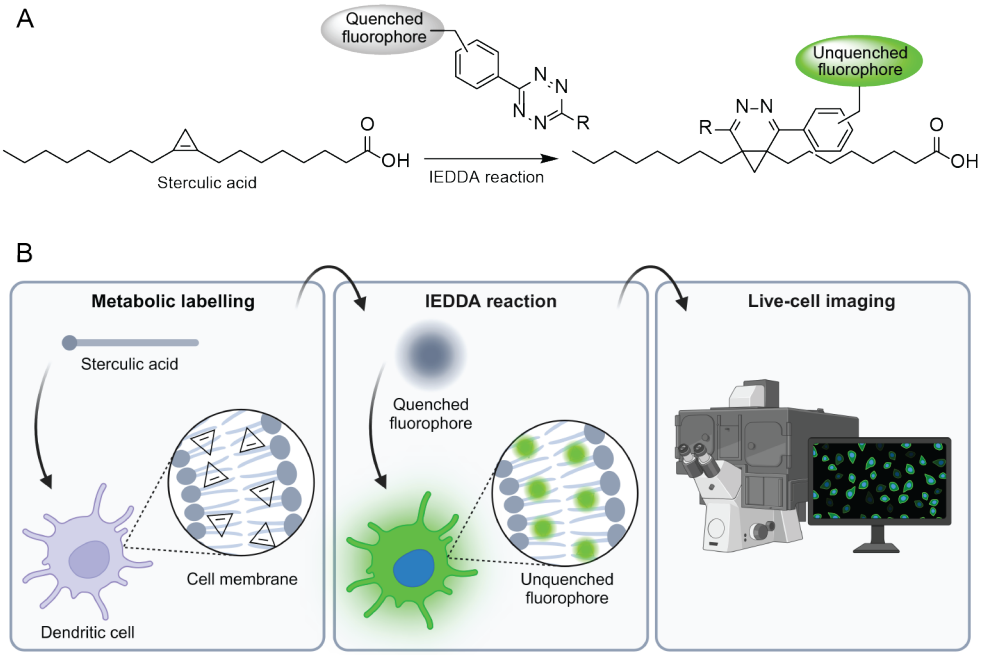

Figure 1: *Schematic overview of* ***A)*** *the inverse electron-demand Diels-Alder (IEDDA) reaction between sterculic acid and a quenched tetrazine-fluorophore conjugate.* ***B)*** *the approach to label dendritic cells with sterculic acid, followed by an IEDDA reaction with tetrazine-fluorophore conjugates to allow for live-cell confocal imaging. The figure is partially made with BioRender.*

Results & Discussion

To assess whether StA could be used in a live-cell IEDDA reaction, a library of tetrazine-conjugated turn-on fluorophores was designed and synthesised by Dr. Merel van de Plassche (Figure 2). The full description of the synthesis and characterisation of all compounds can be found in the publication by Bertheussen et al.[47] Tetrazines have a broad absorption spectrum, which peaks around 515 nm, meaning it can efficiently quench fluorescent dyes of wavelengths ≤ 550 nm via fluorescence resonance energy transfer (FRET).[48,49] Therefore, tetrazine-fluorophore conjugates are so-called turn-on fluorophores, where their fluorescent intensity increases upon ligation, and their reaction with StA can be readily quantified. Two different green fluorophores, BODIPY and Alexa Fluor 488 (AF488) were selected, and ligated to three differently substituted tetrazines (H-, methyl- or pyridyl-substituted), because of the spectrum of reactivity and stability they covered.[50] Additionally, the tetrazines were attached to the BODIPY core at two different distances, as previous research has shown that decreasing the distance between the fluorophore and the tetrazine can improve the quenching effect.[51,52] It has been suggested that the improved quenching effect occurs via an alternate mechanism, through-bond energy transfer (TBET), and not FRET.[52] Photophysical characterisations of the tetrazine-fluorophore conjugates **1-8** can be found in Figure S1 and Table S1.

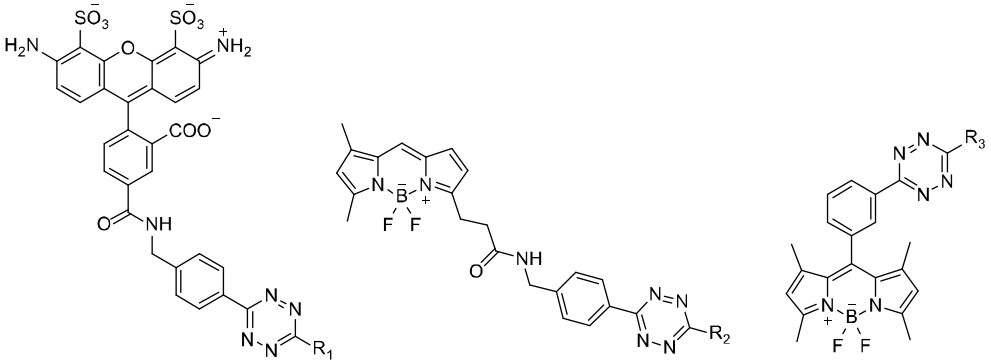

Figure 2: *Structures of tetrazine-fluorophore conjugates **1-8** that were synthesised by Dr. Merel van de Plassche (full synthesis is described in the publication by Bertheussen et al.[47])*

To investigate the fluorescence turn-on of the synthesised fluorophores **1**-**8** upon reaction with StA, the fluorophores were incubated with StA in either PBS, DMSO/H_2O (1:1, v/v) or complete RPMI 1640 medium augmented with 10% fetal calf serum, and the fluorescent signal was measured over time (Figures 3 and S2). In line with previous reports, the two BODIPY-tetrazine conjugates **7** and **8** showed the highest turn-on ratio in PBS, followed by BODIPY FL-tetrazine conjugates **4** and **5**.[51,52] It was also found that H-substituted tetrazine **6,** and pyridyl-substituted tetrazines **5** and **8** reacted faster than methyl-substituted tetrazines **4** and **7**, in agreement with the observations of the Hilderbrand group.[53] This is also reflected in the second-order rate constant for these reactions, which are calculated for tetrazines **4**-**5** and **7**-**8** that display turn-on effects in PBS (Table S1). Surprisingly the H-substituted tetrazine **6** showed little turn-on in PBS. It has previously been suggested that H-substituted tetrazines can be too unstable to be used in biological applications.[54] Stability assessment of the tetrazine library in PBS (Figure S3A) indeed confirmed that **6** was prone to degradation over time. It was therefore possible that the reaction between StA and **6** cannot go to completion because of competition with hydrolytic degradation and unquenching of the H-substituted tetrazine. This is further supported by the observation that the relative fluorescent intensity (RFU) of tetrazines **1**-**3** and **6**, all showing little turn-on in PBS, at the starting point is high compared to the maximum RFU measured (Figure S3B). Also, tetrazines **1** and somewhat **2** show decreased stability over time, which could partially explain their low turn-on ratios. However, all AF488-tetrazine conjugates **1**-**3** showed very little quenching by the pendant tetrazines (Figure 3). This is difficult to explain, as non-sulfonated analogues such as difluorinated-fluorescein are reported to show good turn-on.[51] A possible explanation for this could either be poor resonance energy transfer[48], photo-induced electron transfer[55], or “energy transfer to a dark state” that have been reported to be important quenching mechanisms for longer bond-length tetrazines.[56] Some loss of fluorescence, likely due to photobleaching, was also observed for **7** and **8.** In DMSO/H_2O or complete medium little-to-no turn-on was observed for all the fluorophores (Figure S2). For turn-on measurements in DMSO/H_2O, this could

be explained by the high intrinsic fluorescence for almost all the fluorophores (except **8**) in the solvent, as shown in Figure S3B.

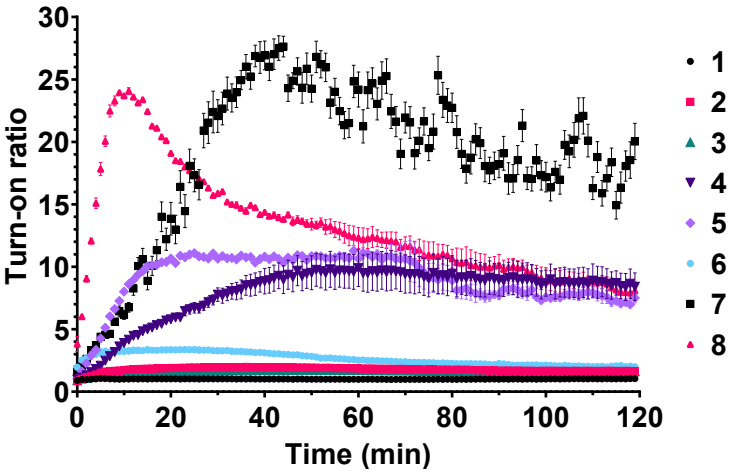

Figure 3: *Average turn-on ratio of tetrazine-fluorophore conjugates **1-8** upon reaction with sterculic acid in PBS at 25 °C. All conditions were measured in triplicate, and standard deviations are indicated.*

Due to the capricious turn-on behaviour of the tetrazine-fluorophore conjugates, all of conjugates were assessed in a live-cell imaging experiment with StA (Figure S4). In contrast to the cell-free medium results discussed above, **4**-**8** all exhibited successful ligation after uptake of StA by DC2.4 dendritic cells[57]. This cell line was chosen due to its excellent imaging properties and previous experience in using it as an *in vitro* model cell line for optimising bioorthogonal chemistry.[58] The Alexa Fluor-based dyes **1**-**3** were unable to react with StA in live cells. This is likely due to the hydrophilic nature of these fluorophores, caused by their sulfonation pattern, not allowing them to diffuse over the hydrophobic plasma membrane. This is in line with previously reported data.[59,60] Fluorophore **7** showed the brightest labelling with the lowest background fluorescence, allowing for imaging at lower laser intensities. As this leads to less bleaching of the sample, **7** was deemed to be the best fluorophore for live-cell imaging (Figure 4A). During live-cell labelling, H-, methyl- and pyridyl-substituted tetrazines give equally bright fluorescent signals, and the substituent on the tetrazine core thereby appears to not make a difference.

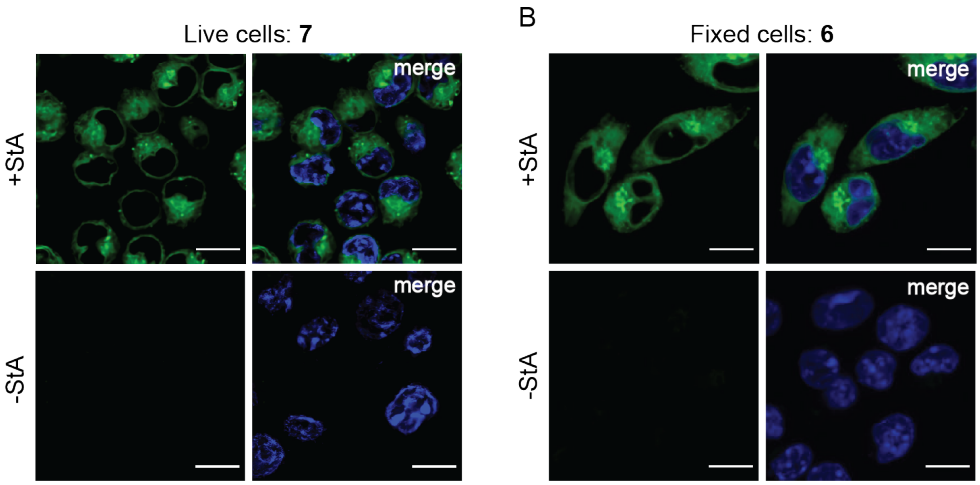

Figure 4: *Confocal imaging of DC2.4 cells incubated with sterculic acid (+StA, 50 µM) or without the probe (-StA).* ***A)*** *Live-cell imaging of labelled cells visualised with fluorophore* ***7*** *(5 µM).* ***B)*** *Fixed-cell imaging of labelled cells visualised with* ***6*** *(5 µM). The samples were washed after metabolic incorporation of StA and after ligation with the fluorophore-tetrazines and were imaged at >4 distinct locations in the same well. DNA was counterstained with Hoechst 33342 (blue) for reference. Scale bars represent 10 µm.*

To evaluate whether StA was also able to react with the tetrazine-fluorophore conjugates in fixed cells, the entire fluorophore library was also tested on fixed and permeabilised cells (Figure S5). Consistent with the results found in live cells, fluorophores **4**-**6** were able to visualise the localisation of StA. As opposed to the live-cell imaging, **1**-**3** showed labelling in fixed and permeabilised cells. However, the intensity of the signal of **1** and **2** was too low to be detected at the same laser settings as **4**-**6**. Upon increased laser intensity, these fluorophores also showed signal over background (Figure S6). The signals of **7** and **8** were the brightest of the library, but showed oversaturated spots in fixed cells, which could originate from precipitation of the fluorophores under the reaction conditions. A general trend seen from the tetrazine library in fixed cells is that the H-substituted tetrazines give the brightest signal, followed by the pyridyl tetrazines. Fluorophore **6** was deemed to be the best alternative for fixed cells, due to its bright and consistent labelling (Figures 4B & S5), despite showing low turn-on in PBS (Figure 3). A direct comparison between the turn-on study and cellular imaging is difficult, due to differing conditions in the two situations. In the turn-on study, there is an excess of StA reacting with the fluorophores, whereas the concentration of StA after metabolic incorporation for cellular imaging is the limiting factor, leading to an excess of the fluorophores instead. In addition, unreacted and potentially degraded fluorophore was routinely washed away before imaging, reducing the background signal, while this was not possible for the turn-on study.

In addition to the fluorophore library, StA was also shown to react with the commercially available (sulfo-)Cy5 tetrazine in a similar manner, allowing its use in a fixed-cell confocal imaging experiment (Figure S7). Use of the Cy5 fluorophore shows a similar labelling pattern as described for the other tetrazine-fluorophore

conjugates, even though it has no turn-on effect.

While unreacted fluorophore was routinely washed away from both live- and fixed-cell samples prior to confocal imaging to minimise background signal, sample preparation and preservation, especially for live-cell imaging, would benefit from the reduction of washing steps. Therefore, it was showed that the turn-on effect of fluorophores **4**-**5** and **7**-**8** upon ligation with StA was sufficient for wash-free live-cell imaging without any detectable background signal (Figure S8).

The metabolic fate of StA after uptake is not known, but in both live and fixed cells StA was observed throughout the cells, except for in the nucleus (Figure 4). Since exogenous free fatty acids can be readily incorporated into phospholipids and other cellular lipids via an acyl coenzyme A intermediate[61], this could indicate that StA is incorporated into plasma and organellar membranes. This is in keeping with StA serving as a mimic for oleic acid, which is known to be found ubiquitously in membrane lipids.[62] In fixed cells (Figure 4B), which are displayed as maximum intensity projections, it also appears that the fluorescent signal is stronger in the endoplasmic reticulum (ER). This can be explained by the incorporation of the free fatty acids into phospholipids through Lands' cycle and the Kennedy pathway, which occur mainly at the ER.[63] However, this would need to be verified by co-stain experiments with an ER marker.

Multiplexing of bioorthogonal reactions is growing in popularity, meaning more complex systems can be studied simultaneously.[64] Previous work has, among other things, shown that two CuAAC reactions can be combined in the same sample.[46] Here, it was explored whether the StA ligation could be included in this workflow, allowing three biomolecules to be simultaneously visualised by multimodal fluorescent imaging. DC2.4 cells were metabolically labelled with the alkyne-containing thymidine analogue 5-ethynyl-2'-deoxyuridine (EdU)[65], the azide-containing palmitic acid analogue 15-azidopentadecanoic acid (azido palmitic acid, azPA) and StA, after which the cells were fixed before performing the corresponding bioorthogonal reactions with AZDye 555 azide, AZDye 647 alkyne, and compound **5**, respectively (Figures 5 and S9). The facile inclusion of StA in both live-cell and multi-click workflows – with good signal-to-noise ratios for all three click reactions indicates that StA does not have detectable cross-reactivity with the CuAAC reagents or cellular components. This means that StA can be used in combination with other click chemistries, allowing for the simultaneous study of multiple biomolecules.

As a note of caution, StA has been reported to be an inhibitor of the enzyme stearoyl-CoA desaturase 1 (SCD1) which catalyses the transformation of saturated fatty acids such as stearic or palmitic acid to their monounsaturated counterparts oleic or palmitoleic acid, respectively.[66] Lowered activity of SCD1 has been linked to various cellular responses such as ER stress, autophagy, and apoptosis[66], which in turn poses the question if the addition of StA would be toxic to the cells by its inhibiting effect on SCD1. To ensure that this was not the case, DC2.4 cells were incubated with a concentration range of StA and cell viability after 24 h was measured by 3-(4,5-dimethylthiazol-2-yl)-2,5-diphenyltetrazolium bromide (MTT) assay (Figure S10). No significant decrease of DC2.4 cell viability was observed for concentrations of StA up to 50 μM and at higher concentrations there was no difference with vehicle-induced toxicity. This further strengthens the applicability of StA as a novel

bioorthogonal analogue of oleic acid. Nevertheless, inhibition of SCD1 should be considered in future use StA, and other cyclopropene-modified lipids.

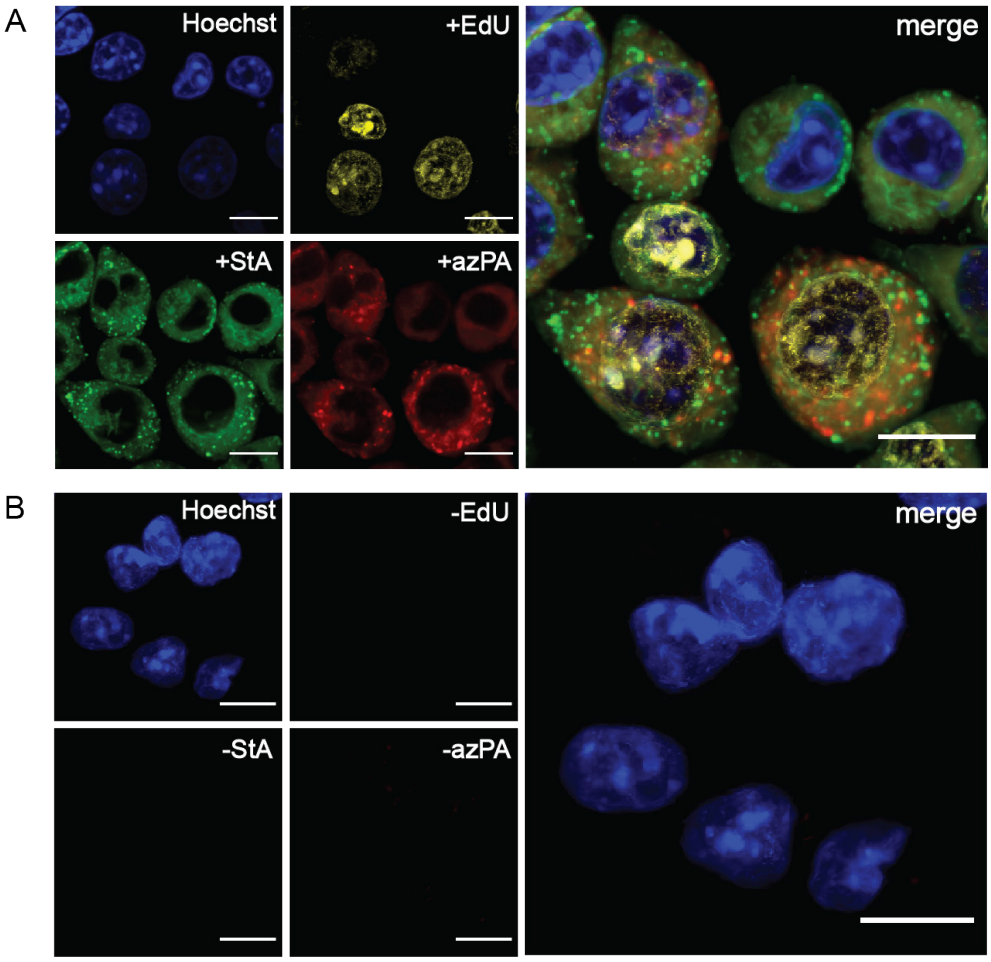

Figure 5: *Confocal imaging of triple-bioorthogonally labelled DC2.4 cells incubated with* ***A)*** *5-ethynyl-2'deoxyuridine (EdU, 10 µM, yellow) for 20 h, followed by sterculic acid (StA, 50 µM, green) and azido palmitic acid (azPA, 100 µM, red) simultaneously for 1 h. The probes were visualised with AZDye 555 azide, compound* ***5****, and AZDye 647 alkyne (all 5 µM), respectively.* ***B)*** *The cells were incubated without probes and treated in the same triple-click manner as described above to show the background signal. The samples were washed between each metabolic incorporation and between each respective bioorthogonal reaction and were imaged at 3 distinct locations in the same well. DNA was counterstained with Hoechst 33342 (blue) for reference. All scale bars represent 10 µm*

Conclusion

Here, the first use of sterculic acid, a non-toxic 1,2-substituted cyclopropene-containing fatty acid, for studying lipids in both live and fixed cells has been reported. The cyclopropene moiety readily reacts with the library of tetrazine-fluorophore conjugates, allowing the study of fatty acid localisation by confocal microscopy. This reaction can occur in a mutually orthogonal manner with two subsequent CuAAC reactions, allowing the study of multiple biomolecules simultaneously. The use of sterculic acid, means that unsaturated lipids can now be visualised using live-cell microscopy; a sorely needed addition to the available tools for these elusive biomolecules.

Acknowledgements

Dr. Thomas Bakkum is acknowledged for his help in setting up the microscopy assays of StA uptake. Dr. Merel van de Plassche is acknowledged for her contribution in synthesising and characterising the tetrazine-fluorophore conjugate library. Prof. Kenneth L. Rock is thanked for his kind gift of the DC2.4 cell line.

Materials & Methods

General. Sterculic acid (#26735) was purchased from Cayman Chemical and stored as 10 mM or 100 mM stock solutions in DMSO at -20°C. Azido palmitic acid (#1346) was purchased from Click Chemistry Tools (now VectorLabs) and stored as 10 mM or 50 mM stock solutions in DMSO at -20°C. 5-ethynyl-2'-deoxyuridine (EdU, #900584) was purchased from Sigma Aldrich and stored as a 10 mM stock solution in DMSO at -20°C. The tetrazine-fluorophore conjugates **1**-**8** were synthesised in-house (as described in the publication by Bertheussen et al.[47]), and were stored as 2 mM stock solutions in DMSO at -20°C. The other fluorophores (sulpho-)Cy5 tetrazine (#1189), AZDye 555 azide (#1287), AZDye 647 alkyne (#1301) were all purchased from Click Chemistry Tools (now VectorLabs), and stored as 2 mM stock solutions in DMSO at -20°C.

Mammalian cell culture. DC2.4 cells were cultured in RPMI 1640 culture medium (Gibco, #31870025) supplemented with 10% FCS, GlutaMAX (2 mM), sodium pyruvate (1 mM), 1x non-essential amino acids (NEAA, Thermo Fisher Scientific), penicillin (100 I.U./mL), streptomycin (50 µg/mL), and 2-mercaptoethanol (50 µM, Thermo Fisher Scientific), and incubated at 37 °C, 5% CO_2. The cells were grown to 70-80% confluency and passaged every 2-3 days by trypsinisation.

Measuring turn-on of the tetrazine-fluorophore conjugates. Dilutions of the fluorophores **1**-**8** (2 µM) and StA (10 µM, Cayman Chemical) were prepared in three solvents; PBS, DMSO/H_2O (1:1, v/v), and phenol red-free RPMI 1640 culture medium (Thermo Fisher Scientific) supplemented with 10% FCS, GlutaMAX (2 mM), pyruvate (1 mM) and 1x NEAA. The solvents were analysed one at a time by adding 50 µL of the fluorophore dilutions in triplicate in a black 96-well plate, followed by addition of 50 µL StA dilution or 50 µL only solvent (negative control). This gives final concentrations of 1 µM fluorophore, and 5 µM StA. The plate was immediately scanned for fluorescence on a CLARIOstar plate reader (BMG LABTECH) with excitation/emission at 477-14/530-40 and dichroic filter 497. Fluorescence was measured once every 60 sec for 120 min. The results were processed and plotted in GraphPad Prism version 9.3.1 showing the turn-on ratio between the sample and negative control, as an average of the triplicated samples and with indicated standard deviations.

Reaction kinetics between tetrazine-fluorophore conjugates and sterculic acid. To calculate the second-order rate constants (k_2) for the reaction between tetrazines **1**-**8** and StA, the data assembled for the turn-on measurements (described earlier) were used and a previously published procedure was followed.[67] After having subtracted background fluorescence values from the data, each curve was capped at its initial plateau, after the exponential phase, to prevent photobleaching from affecting the calculations. Each replicate (n=3) was processed separately for the whole analysis. Since the experiment was performed under pseudo first-order conditions, the pseudo first-order rate constant k_1' was determined using the 'One phase decay' regression in GraphPad Prism version 9.3.1 on the data points. The second-order rate constant was then calculated as $k_2 = k_1'/c_{StA}$, and standard deviations were calculated for the replicates.

Preparation of live-cell samples. For microscopy, $6x10^5$ DC2.4 cells were seeded

per well on an 8-well chamber slide (Ibidi) and allowed to attach for 2 h. The cells were incubated with StA (50 µM) or no probe (negative control) for 1 h in complete medium (as described above) with 0.1% fatty acid-free BSA (Sigma Aldrich) instead of FCS. Cells were washed with fresh medium x3, followed by incubation with the respective fluorophores **1**-**8** from the tetrazine library (5 µM) in complete medium for 1 h. For Figures 4A and S4, the cells were washed with fresh medium x3 after fluorophore ligation to remove unreacted probe, and DNA was counterstained with Hoechst 33342 (5 µg/mL, Sigma Aldrich) in PBS for 5-10 min followed by washing with PBS x3. For Figure S8, labelling medium was aspirated and DNA was immediately counterstained with Hoechst 33342 (5 µg/mL, Sigma Aldrich) in PBS for 5-10 min without washing steps. Each incubation step was done at 37 °C, 5% CO_2. All samples were directly imaged in phenol red-free DMEM (Sigma Aldrich) supplemented with GlutaMAX (2 mM), sodium pyruvate (1 mM), penicillin (100 I.U./mL), and streptomycin (50 µg/mL), by confocal microscopy (see below).

Preparation of fixed-cell samples. The same protocol was followed as for live-cell imaging (described above) until the point of incubation with StA, after which the cells were fixed with 4% paraformaldehyde (PFA) in PBS for 30 min at room temperature. After fixation the cells were washed with PBS followed by glycine (20 mM) in PBS to quench unreacted aldehyde. The cells were permeabilised with 0.01% saponin in PBS for 20 min and washed with PBS x2. The permeabilised sample was incubated with the tetrazine-fluorophore conjugate library (**1**-**8**, 5 µM) or (sulpho-)Cy5 tetrazine (20 µM) in PBS for 1 h, followed by washing with PBS x2 and blocking with 1% BSA in PBS for 30 min. DNA was counterstained with Hoechst 33342 (2 µg/mL) in PBS for 5-10 min. The incubation steps were done at room temperature and separated by intermediate washing steps with PBS. The cells were then imaged directly in glycerol/DABCO mounting medium to minimise photo bleaching.

Preparation of triple-labelled sample. For microscopy, $6x10^5$ DC2.4 cells were seeded per well on an 8-well chamber slide (Ibidi) and allowed to attach for 3 h. The triple metabolic labelling started with incubating the cells with EdU (10 µM) in complete medium for 20 h, followed by washing with PBS x2. Then a metabolic label cocktail containing StA (50 µM) and azido palmitic acid (100 µM) in medium with 0.1% fatty acid-free BSA (Sigma Aldrich) instead of FCS, was added to the sample and it was incubated for 1 h. The sample was washed with fresh medium x1 and PBS x1 and fixed in 2% PFA in 0.1M phosphate buffer pH 7.2 at room temperature overnight. Fixation solution was aspirated, and sample was washed with PBS and glycine (20 mM) in PBS, and permeabilised with 0.01% saponin in PBS for 20 min. The sample was first reacted with fluorophore **5** (5 µM) in PBS for 1 h, followed by AZDye 555 azide (5 µM) in copper-click cocktail (1 mM $CuSO_4$, 10 mM sodium ascorbate, 1 mM THPTA ligand, 10 mM amino-guanidine, 0.1 M HEPES pH 7.2) for 1 h and finally AZDye 647 alkyne (5 µM) in copper-click cocktail for 1 h. All bioorthogonal reactions were performed with intermediate washing steps with PBS x2, and after the reactions unreacted fluorophores were blocked with 1% BSA in PBS for 30 min. DNA was counterstained with Hoechst 33342 (2 µg/mL) in PBS for 5-10 min and the sample was imaged directly in glycerol/DABCO mounting medium.

Confocal microscopy. All slides were imaged on an AR1 HD25 confocal microscope (Nikon), equipped with a Ti2-E inverted microscope, LU-NV Series laser unit, and CFI Plan Apo Lambda 100x/1.45 oil objective. Hoechst, the tetrazine-fluorophore

conjugates, AZDye 555, and AZDye 647 and (sulpho-)Cy5 were excited using the 405 nm, 488 nm, 561 nm, and 647 nm laser lines, respectively, and images were acquired using the Resonant scanner and DU4 detector (495LP (450/50), 560LP (525/50), 640LP (595/50)). Poisson noise was immediately removed from the images by the built-in Nikon Denoise.ai software. Z-stacks were acquired from the fixed-cell and triple-labelled samples with 0.20-micron steps and are all presented as maximum intensity projections. Brightness and contrast were adjusted for all samples using ImageJ. Brightness and contrast were adjusted identically for samples that are directly compared to each other to make sure the relative intensity between the samples remain the same.

Assessing the cytotoxicity of sterculic acid. A 3-(4,5-dimethylthiazol-2-yl)-2,5-diphenyltetrazolium bromide (MTT) assay was performed to ensure the concentration of StA used in the following experiments was not cytotoxic. In a 96-well plate (Sarstedt), $1x10^5$ DC2.4 cells were seeded per well and allowed to attach for 2 h. Serial dilutions (1:2) of StA (stock concentration 10 mM in DMSO) in complete medium, in the range of 12.5-200 µM, were prepared. These were added in triplicate, together with the appropriate controls and blanks and incubated for 24 h. The cells were spun down (300 g, 5 min) and the culture medium was replaced with complete medium containing MTT (0.5 mg/mL). The plate was incubated for 3 h and spun down at (300 g, 5 min) before the medium was aspirated. The formed formazan crystals were dissolved in DMSO, and the plate was incubated for 2 min with 400 rpm shaking. All incubation steps were done at 37 °C, 5% CO_2. Absorbance was measured at 570 nm on a CLARIOstar plate reader (BMG LABTECH). The data were normalised against cells that had no StA added, and the normalised standard deviations are given.

Supplementary Figures & Tables

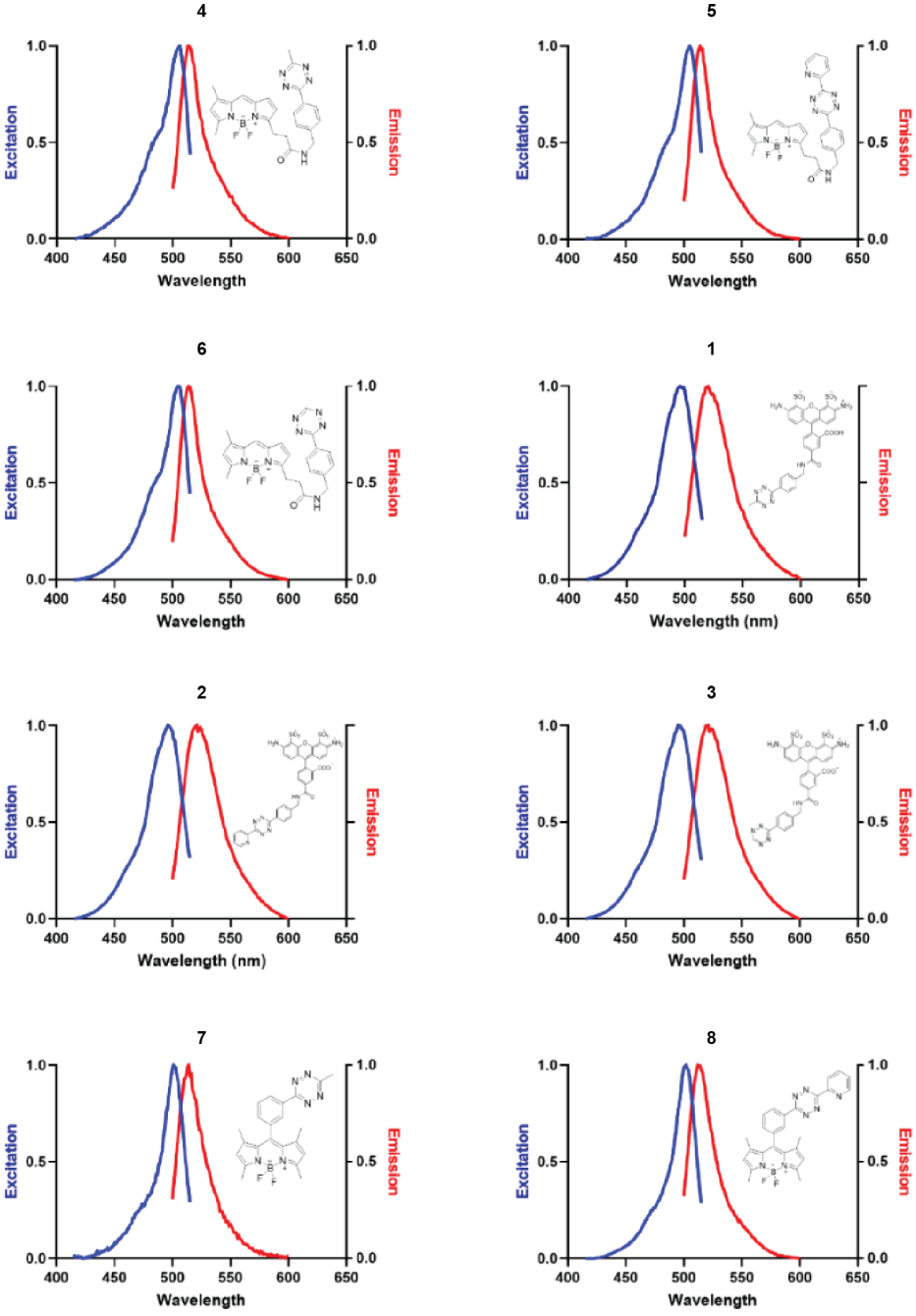

Figure S1: *Normalised excitation and emission spectra of fluorophores* ***1-8*** *measured at a final concentration of 1 µM in PBS on a CLARIOstar plate reader.*

Table S1: *Characterisations of the photophysical properties of tetrazine-fluorophore conjugates* ***1-8****, and their kinetics upon reaction with sterculic acid. Absorption maximum (Λ_{abs}) and extinction coefficient (E_{max}) of the tetrazine-fluorophore conjugates (1 µM) in DMSO/H_2O (1:1) and PBS. Second-order rate constants (k_2) for the conjugates (1 µM) upon reaction with sterculic acid (5 µM) in PBS.*

Fluorophore	Λ_{abs} (nm) DMSO/H_2O (1:1)	E_{max} ($M^{-1}cm^{-1}$) DMSO/H_2O (1:1)	Λ_{abs} (nm) PBS	E_{max} ($M^{-1}cm^{-1}$) PBS	k_2 ($M^{-1}s^{-1}$)
1	500	58000	492	48000	ND
2	500	45000	492	36000	ND
3	500	39000	494	39000	ND
4	506	60000	506	34000	125 ± 41
5	508	28000	506	16000	660 ± 28
6	506	43000	506	24000	ND
7	500	59000	500	26000	658 ± 14
8	502	82000	500	26000	328 ± 36

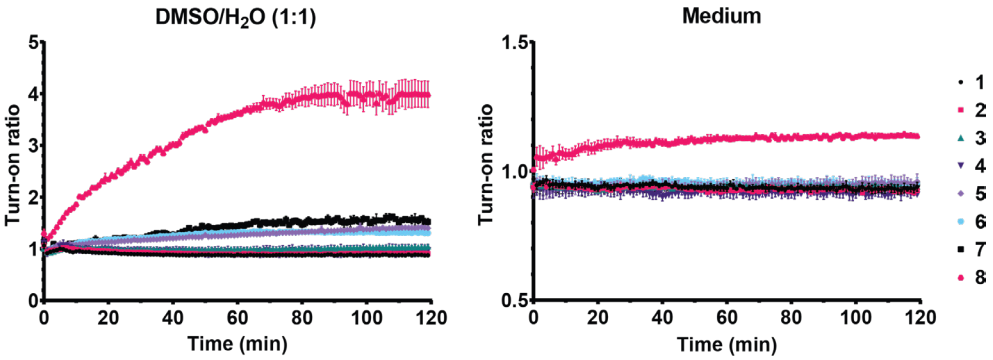

Figure S2: *Average turn-on ratio of tetrazine-fluorophore conjugates* ***1-8*** *upon reaction with sterculic acid in DMSO/H_2O (1:1, v/v) or complete medium at 25°C. All conditions were measured in triplicate, and standard deviations are indicated.*

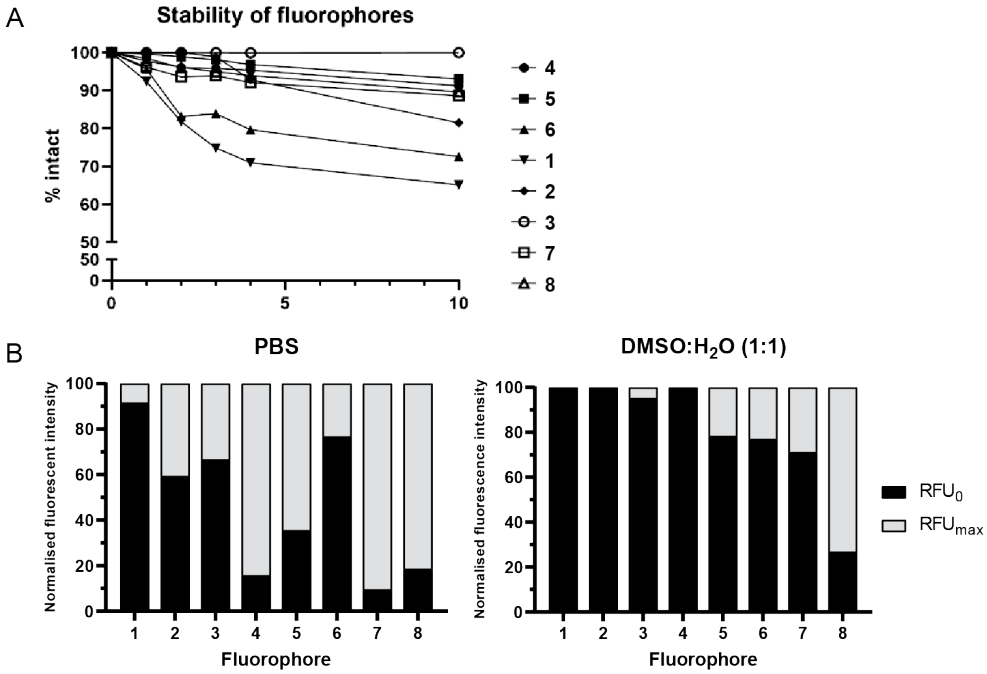

Figure S3: *Further insight into the stability and turn-on ability of tetrazine-fluorophore conjugates* ***1-8****.* ***A)*** *Stability of the fluorophores (10 µM) in PBS at RT for 10 h as measured by LCMS. The integral of the peak at 0 min was set as 100%.* ***B)*** *Each fluorophore (1 µM) was reacted with sterculic acid (5 µM) in PBS and DMSO:H_2O (1:1) at RT, and the fluorescent intensity at the start-point of measurement (RFU_0) is compared to the maximum fluorescent intensity (RFU_{max}). RFU_{max} for each fluorophore is set to 100%.*

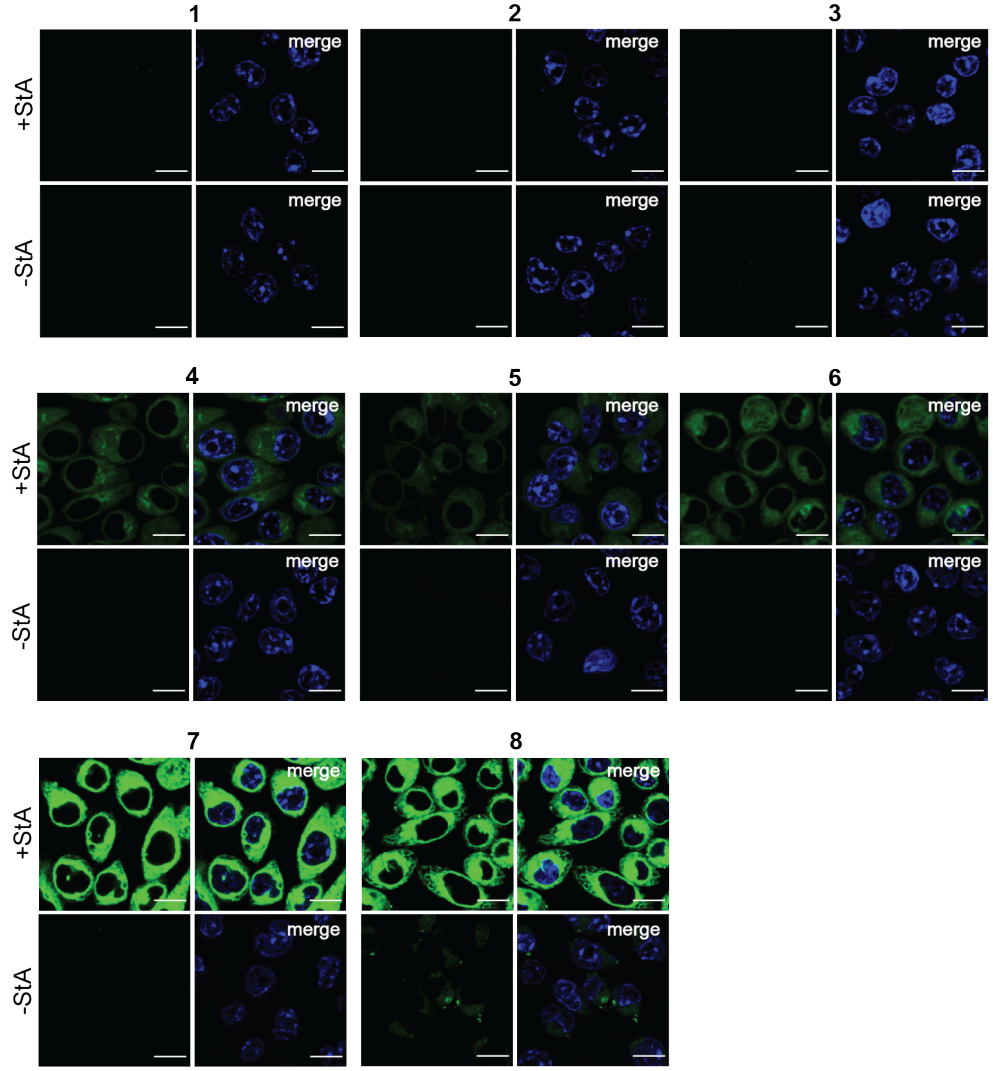

Figure S4: *Confocal live-cell imaging of tetrazine-fluorophore conjugate library (**1**-**8**). DC2.4 cells were incubated with sterculic acid (+StA, 50 µM) or no probe (-StA) for 1 h, followed by click reaction with the respective fluorophore (all 5 µM) for 1 h. Images are presented as single slices. All samples were routinely washed after metabolic incorporation of sterculic acid and after ligation with the fluorophores and were imaged with minimum 4 technological replicates. DNA was counterstained with Hoechst 33342. All scale bars represent 10 µm.*

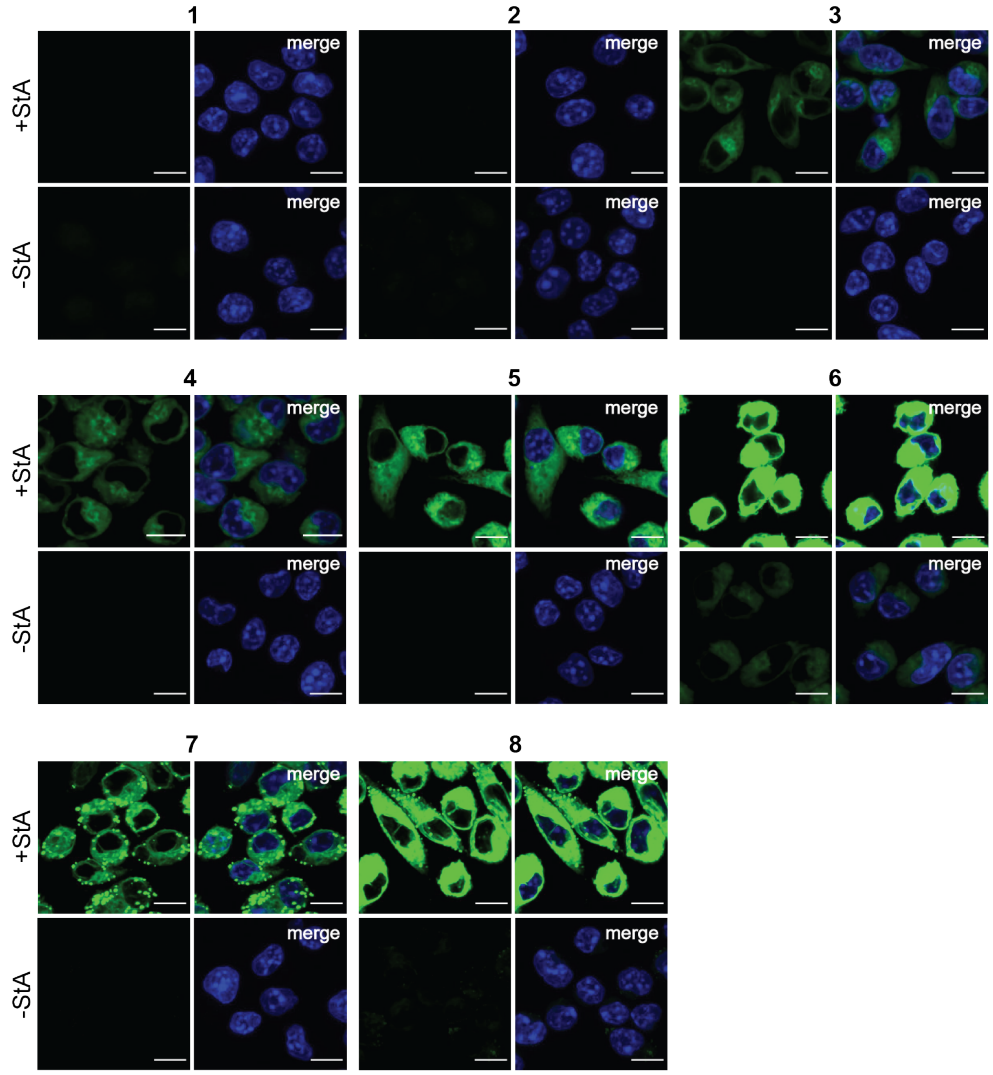

Figure S5: *Confocal fixed-cell imaging of tetrazine-fluorophore conjugate library (**1**-**8**). DC2.4 cells were incubated with sterculic acid (+StA, 50 µM) or no probe (-StA) for 1 h, fixed and permeabilised, followed by click reaction with the respective fluorophore (all 5 µM) for 1 h. Images are presented as maximum intensity projections of z-stacks. All samples were routinely washed after metabolic incorporation of sterculic acid and after ligation with the fluorophores and were imaged with minimum 4 technological replicates. DNA was counterstained with Hoechst 33342. All scale bars represent 10 µm.*

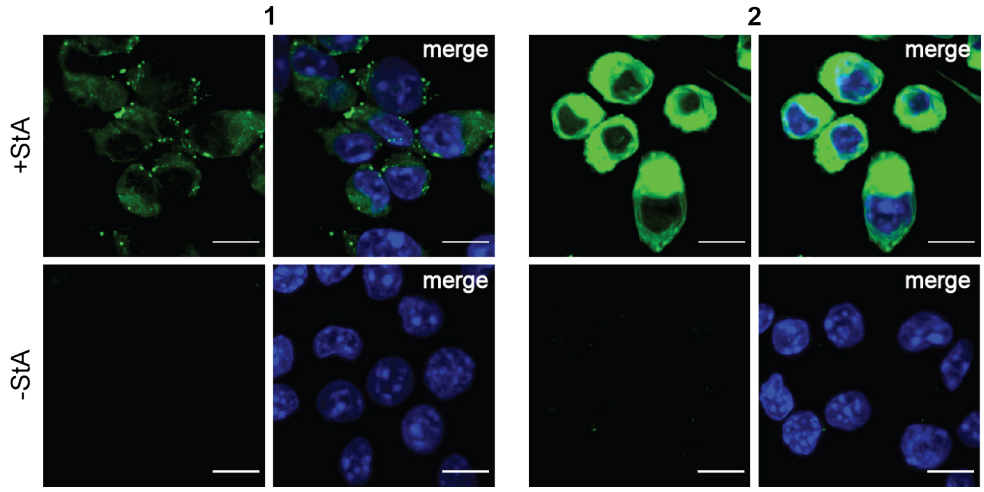

Figure S6: *Confocal fixed-cell imaging of fluorophores* ***1-2*** *with higher laser power. DC2.4 cells were incubated with sterculic acid (+StA, 50 µM) or no probe (-StA) for 1 h, fixed and permeabilised, followed by click reaction with the respective fluorophore (5 µM) for 1 h. Images are presented as maximum intensity projections of z-stacks. All samples were washed after metabolic incorporation of sterculic acid and after ligation with the fluorophores. DNA was counterstained with Hoechst 33342 (blue). All scale bars represent 10 µm.*

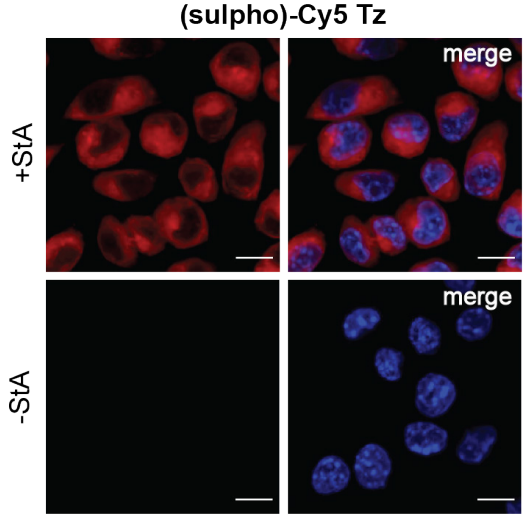

Figure S7: *Confocal fixed-cell imaging with (sulpho-)Cy5 tetrazine. DC2.4 cells were incubated with sterculic acid (+StA, 50 µM) or no probe (-StA) for 1 h, fixed and permeabilised, followed by click reaction with (sulpho-)Cy5 tetrazine (20 µM) for 1 h. Images are presented as maximum intensity projections of z-stacks. All samples were routinely washed after metabolic incorporation of sterculic acid and after ligation with the fluorophores and were imaged with 4 technological replicates. DNA was counterstained with Hoechst 33342 (blue). All scale bars represent 10 µm.*

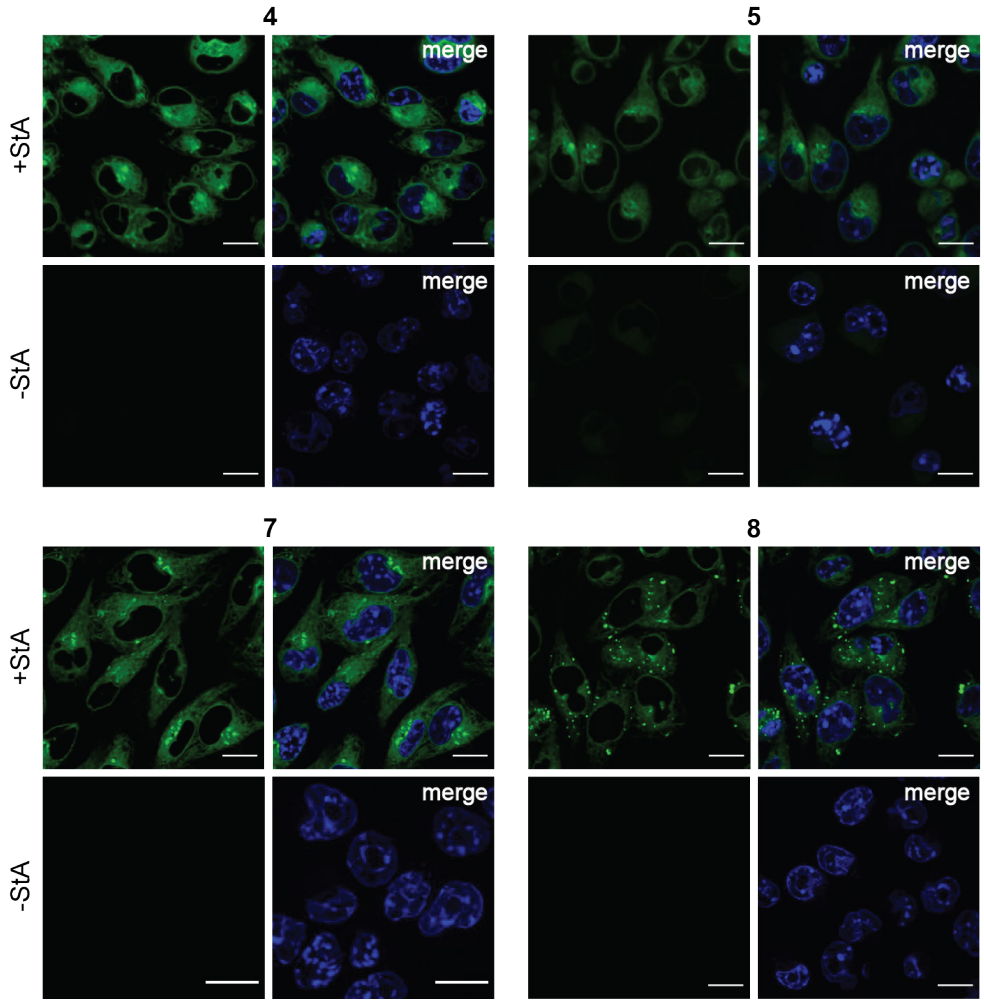

Figure S8: *Confocal live-cell imaging without washing steps after ligation between sterculic acid and fluorophores* ***4*****-****5*** *and* ***7*****-****8****. DC2.4 cells were incubated with sterculic acid (+StA, 50 µM) or no probe (-StA) for 1 h, followed by a wash step to remove excess sterculic acid, and click reaction with the respective fluorophore (all 5 µM) for 1 h. DNA was counterstained with Hoechst 33342, and samples were imaged directly without further wash steps. Images are presented as single slices and were imaged with minimum 3 technological replicates. Fluorophores* ***7*****-****8*** *were imaged at a lower laser intensity than* ***4*****-****5****. DNA was counterstained with Hoechst 33342 (blue). All scale bars represent 10 µm.*

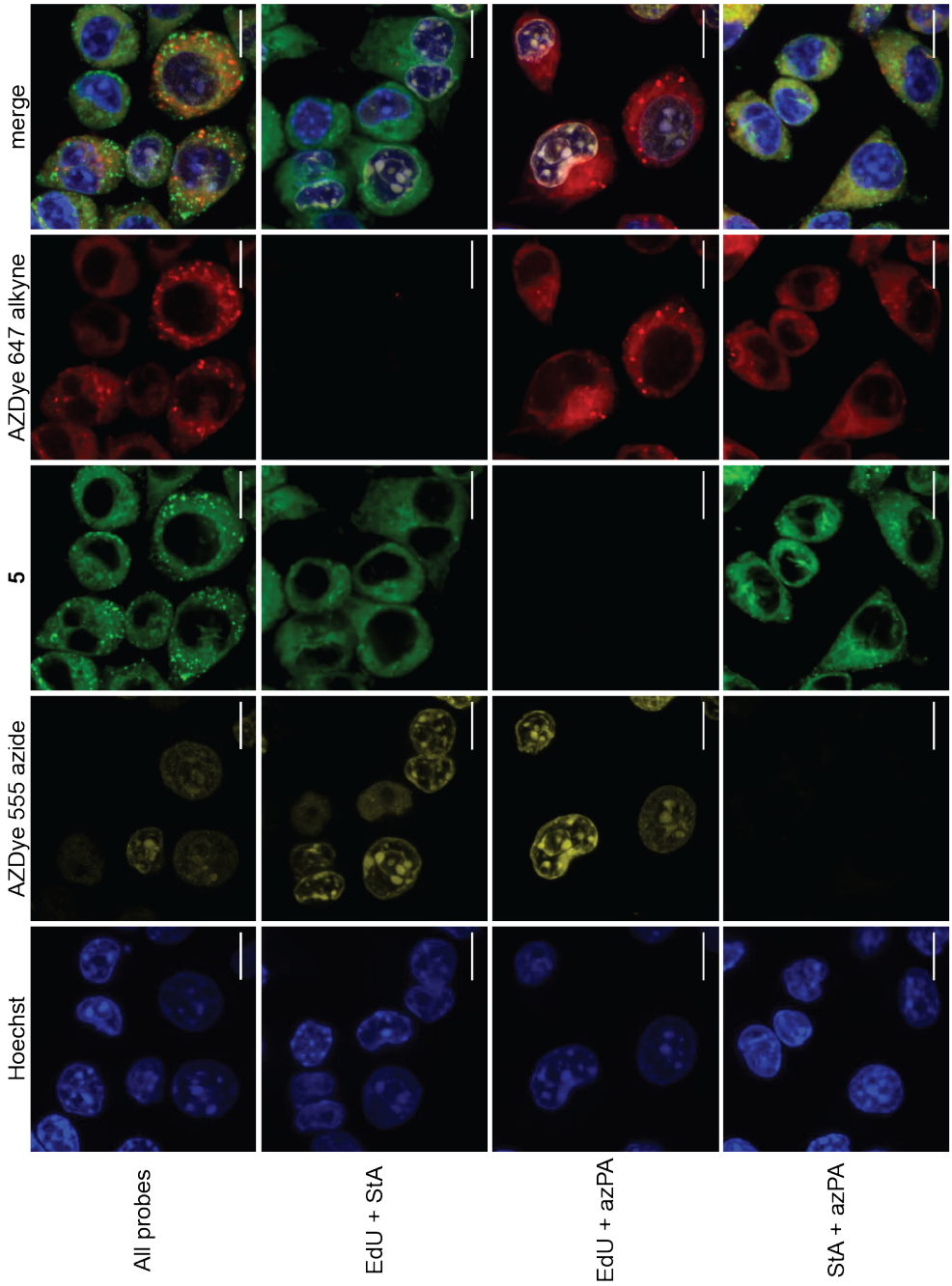
merge
AZDye 647 alkyne
5
AZDye 555 azide
Hoechst
All probes
EdU + StA
EdU + azPA
StA + azPA

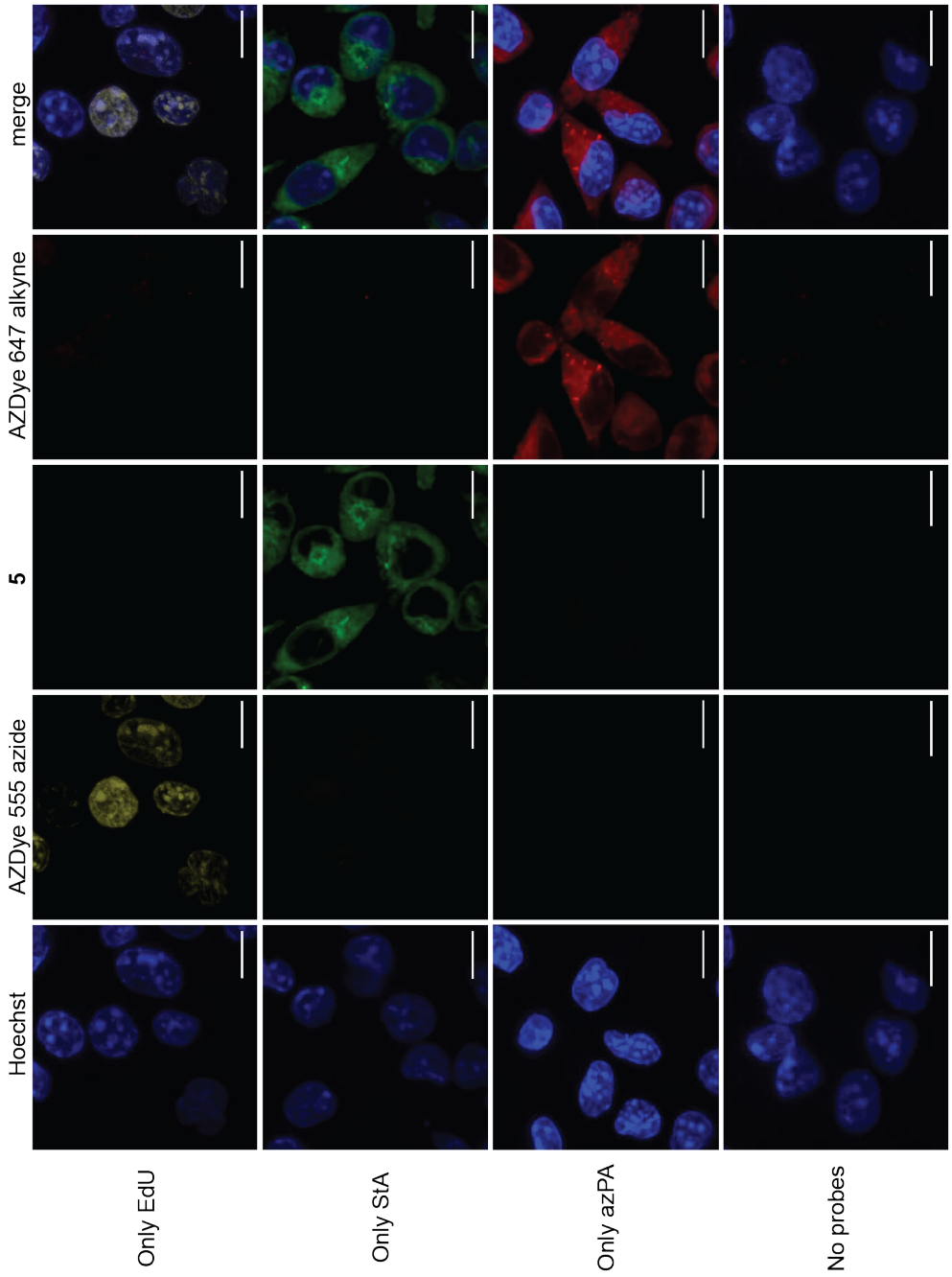
Hoechst
AZDye 555 azide
5
AZDye 647 alkyne
merge
Only EdU
Only StA
Only azPA
No probes

Figure S9: *Confocal imaging of triple-labelled sample with all respective controls. DC2.4 cells were incubated with EdU (10 μM) for 20 h, followed by sterculic acid (StA, 50 μM) and azido palmitic acid (azPA, 100 μM) for 1 h, or the respective combination of these probes. The cells were then fixed and permeabilised, followed by a triple-click strategy. All samples were first clicked with fluorophore* ***5*** *(5 μM) for 1 h, followed by two subsequent CuAAC reactions with AZDye 555 azide (5 μM) and AZDye 647 alkyne (5 μM) for 1 h each. All samples were routinely washed between each metabolic incorporation and between each respective bioorthogonal reaction and were imaged with 3 technological replicates. Images are presented as maximum intensity projections of z-stacks. DNA was counterstained with Hoechst 33342 (blue) as a reference. All scale bars represent 10 μm.*

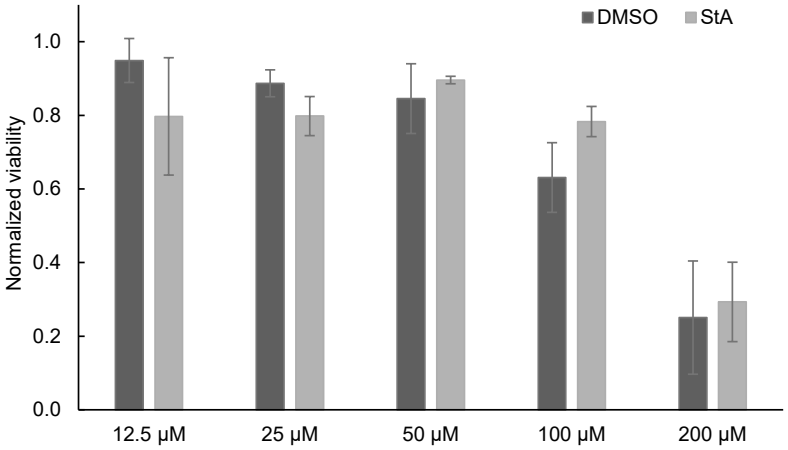

Figure S10: *Toxicity of sterculic acid (StA), as assessed by MTT assay. DC2.4 cells were incubated with given concentrations (μM) of StA in DMSO (labelled StA), or the corresponding amount of DMSO (ranging from 0.125-2%) without StA (labelled DMSO) for 24 h. Absorbance was measured at 570 nm. Absorbance values were measured in triplicate and normalised to an untreated control. Standard deviations are indicated.*

References

1. Houten, S. M. & Wanders, R. J. A. A general introduction to the biochemistry of mitochondrial fatty acid β-oxidation. *Journal of inherited metabolic disease* **33**, 469–477 (2010).
2. van Meer, G., Voelker, D. R. & Feigenson, G. W. Membrane lipids: where they are and how they behave. *Nature Reviews Molecular Cell Biology* **9**, 112–124 (2008).
3. Resh, M. D. Fatty acylation of proteins: The long and the short of it. *Progress in Lipid Research* **63**, 120–131 (2016).
4. Wymann, M. P. & Schneiter, R. Lipid signalling in disease. *Nature Reviews Molecular Cell Biology* **9**, 162–176 (2008).
5. Bumpus, T. W. & Baskin, J. M. Greasing the Wheels of Lipid Biology with Chemical Tools. *Trends Biochem Sci* **43**, 970–983 (2018).
6. Ticho, A. L. *et al.* S-acylation modulates the function of the apical sodium-dependent bile acid transporter in human cells. *Journal of Biological Chemistry* **295**, 4488–4497 (2020).
7. Thinon, E., Percher, A. & Hang, H. C. Bioorthogonal Chemical Reporters for Monitoring Unsaturated Fatty-Acylated Proteins. *ChemBioChem* **17**, 1800–1803 (2016).
8. Pérez, A. J. & Bode, H. B. ω-Azido fatty acids as probes to detect fatty acid biosynthesis, degradation, and modification. *J Lipid Res* **55**, 1897–1901 (2014).
9. Kostiuk, M. A. *et al.* Identification of palmitoylated mitochondrial proteins using a bio-orthogonal azido-palmitate analogue. *The FASEB Journal* **22**, 721–732 (2008).
10. Charron, G. *et al.* Robust Fluorescent Detection of Protein Fatty-Acylation with Chemical Reporters. *J Am Chem Soc* **131**, 4967–4975 (2009).
11. Thiele, C. *et al.* Tracing Fatty Acid Metabolism by Click Chemistry. *ACS Chem Biol* **7**, 2004–2011 (2012).
12. Jao, C. Y., Roth, M., Welti, R. & Salic, A. Metabolic labeling and direct imaging of choline phospholipids in vivo. *Proceedings of the National Academy of Sciences* **106**, 15332–15337 (2009).
13. Jao, C. Y., Roth, M., Welti, R. & Salic, A. Biosynthetic Labeling and Two-Color Imaging of Phospholipids in Cells. *ChemBioChem* **16**, 472–476 (2015).
14. Garrido, M., Abad, J. L., Fabriàs, G., Casas, J. & Delgado, A. Azide-Tagged Sphingolipids: New Tools for Metabolic Flux Analysis. *ChemBioChem* **16**, 641–650 (2015).
15. Jao, C. Y. *et al.* Bioorthogonal Probes for Imaging Sterols in Cells. *ChemBioChem* **16**, 611–617 (2015).
16. Hofmann, K. *et al.* A novel alkyne cholesterol to trace cellular cholesterol metabolism and localization. *Journal of Lipid Research* **55**, 583–591 (2014).
17. Rakers, L. *et al.* Addressable Cholesterol Analogs for Live Imaging of Cellular Membranes. *Cell Chemical Biology* **25**, 952–961 (2018).
18. Hang, H. C., Wilson, J. P. & Charron, G. Bioorthogonal Chemical Reporters for Analyzing Protein Lipidation and Lipid Trafficking. *Acc Chem Res* **44**, 699–708 (2011).
19. Liang, D. *et al.* A real-time, click chemistry imaging approach reveals stimulus-specific subcellular locations of phospholipase D activity. *Proceedings of the National Academy of Sciences* **116**, 15453–15462 (2019).
20. Pérez, A. J. & Bode, H. B. “Click Chemistry” for the Simple Determination of Fatty-Acid Uptake and Degradation: Revising the Role of Fatty-Acid Transporters.

ChemBioChem **16**, 1588–1591 (2015).

21. Suazo, K. F., Park, K.-Y. & Distefano, M. D. A Not-So-Ancient Grease History: Click Chemistry and Protein Lipid Modifications. *Chemical Reviews* **121**, 7178–7248 (2021).
22. Rigolot, V., Biot, C. & Lion, C. To View Your Biomolecule, Click inside the Cell. *Angewandte Chemie International Edition* **60**, 23084–23105 (2021).
23. van Geel, R., Pruijn, G. J. M., van Delft, F. L. & Boelens, W. C. Preventing Thiol-Yne Addition Improves the Specificity of Strain-Promoted Azide–Alkyne Cycloaddition. *Bioconjugate Chemistry* **23**, 392–398 (2012).
24. Blackman, M. L., Royzen, M. & Fox, J. M. Tetrazine ligation: fast bioconjugation based on inverse-electron-demand Diels-Alder reactivity. *J Am Chem Soc* **130**, 13518–13519 (2008).
25. Devaraj, N. K., Weissleder, R. & Hilderbrand, S. A. Tetrazine-Based Cycloadditions: Application to Pretargeted Live Cell Imaging. *Bioconjug Chem* **19**, 2297–2299 (2008).
26. Oliveira, B. L., Guo, Z. & Bernardes, G. J. L. Inverse electron demand Diels–Alder reactions in chemical biology. *Chem. Soc. Rev.* **46**, 4895–4950 (2017).
27. Row, R. D. & Prescher, J. A. Constructing New Bioorthogonal Reagents and Reactions. *Acc Chem Res* **51**, 1073–1081 (2018).
28. Erdmann, R. S. *et al.* Super-Resolution Imaging of the Golgi in Live Cells with a Bioorthogonal Ceramide Probe. *Angewandte Chemie International Edition* **53**, 10242–10246 (2014).
29. Erdmann, R. S., Toomre, D. & Schepartz, A. STED Imaging of Golgi Dynamics with Cer-SiR: A Two-Component, Photostable, High-Density Lipid Probe for Live Cells. *Methods in molecular biology (Clifton, N.J.)* **1663**, 65–78 (2017).
30. Oliveira, B. L. *et al.* A Minimal, Unstrained S-Allyl Handle for Pre-Targeting Diels–Alder Bioorthogonal Labeling in Live Cells. *Angewandte Chemie International Edition* **55**, 14683–14687 (2016).
31. Yang, J., Šečkutė, J., Cole, C. M. & Devaraj, N. K. Live-Cell Imaging of Cyclopropene Tags with Fluorogenic Tetrazine Cycloadditions. *Angewandte Chemie International Edition* **51**, 7476–7479 (2012).
32. Patterson, D. M., Nazarova, L. A., Xie, B., Kamber, D. N. & Prescher, J. A. Functionalized Cyclopropenes As Bioorthogonal Chemical Reporters. *Journal of the American Chemical Society* **134**, 18638–18643 (2012).
33. Sauer, J. & Heinrichs, G. Kinetik und umsetzungen von 1.2.4.5-tetrazinen mit winkelgespannten und elektronenreichen doppelbindungen. *Tetrahedron Letters* **7**, 4979–4984 (1966).
34. Dowd, P. & Gold, A. The thermal dimerization of cyclopropene. *Tetrahedron Letters* **10**, 85–86 (1969).
35. Cole, C. M., Yang, J., Šečkutė, J. & Devaraj, N. K. Fluorescent Live-Cell Imaging of Metabolically Incorporated Unnatural Cyclopropene-Mannosamine Derivatives. *ChemBioChem* **14**, 205–208 (2013).
36. Morel, O. *et al.* REPRISAL: mapping lignification dynamics using chemistry, data segmentation, and ratiometric analysis. *Plant Physiology* **188**, 816–830 (2022).
37. Šečkutė, J., Yang, J. & Devaraj, N. K. Rapid oligonucleotide-templated fluorogenic tetrazine ligations. *Nucleic Acids Research* **41**, e148–e148 (2013).
38. Nunn, J. R. The structure of sterculic acid. *Journal of the Chemical Society (Resumed)* 313–318 (1952) doi:10.1039/jr9520000313.

39. Ahmad, M. U., Ali, S. M., Ahmad, A., Sheikh, S. & Ahmad, I. Chapter 5 - Carbocyclic Fatty Acids: Chemistry and Biological Properties. in (ed. Ahmad, M. U. B. T.-F. A.) 147–185 (AOCS Press, 2017). doi:https://doi.org/10.1016/B978-0-12-809521-8.00004-0.

40. Greenberg, A. & Harris, J. Cyclopropenoid fatty acids. *Journal of Chemical Education* **59**, 539 (1982).

41. Kumar, P. *et al.* Lipidated cyclopropenes via a stable 3-N spirocyclopropene scaffold. *Tetrahedron Letters* **59**, 3435–3438 (2018).

42. Hu, Y. & Schomaker, J. M. Recent Developments and Strategies for Mutually Orthogonal Bioorthogonal Reactions. *ChemBioChem* **22**, 3254–3262 (2021).

43. Willems, L. I. *et al.* Triple Bioorthogonal Ligation Strategy for Simultaneous Labeling of Multiple Enzymatic Activities. *Angewandte Chemie International Edition* **51**, 4431–4434 (2012).

44. Simon, C. *et al.* One, Two, Three: A Bioorthogonal Triple Labelling Strategy for Studying the Dynamics of Plant Cell Wall Formation In Vivo. *Angewandte Chemie International Edition* **57**, 16665–16671 (2018).

45. Chio, T. I., Gu, H., Mukherjee, K., Tumey, L. N. & Bane, S. L. Site-Specific Bioconjugation and Multi-Bioorthogonal Labeling via Rapid Formation of a Boron–Nitrogen Heterocycle. *Bioconjugate Chemistry* **30**, 1554–1564 (2019).

46. Bakkum, T. *et al.* Bioorthogonal Correlative Light-Electron Microscopy of Mycobacterium tuberculosis in Macrophages Reveals the Effect of Antituberculosis Drugs on Subcellular Bacterial Distribution. *ACS Central Science* **6**, 1997–2007 (2020).

47. Bertheussen, K. *et al.* Live-Cell Imaging of Sterculic Acid—a Naturally Occurring 1,2-Cyclopropene Fatty Acid—by Bioorthogonal Reaction with Turn-On Tetrazine-Fluorophore Conjugates. *Angewandte Chemie International Edition* **61**, (2022).

48. Beliu, G. *et al.* Bioorthogonal labeling with tetrazine-dyes for super-resolution microscopy. *Communications Biology* **2**, 261 (2019).

49. Wieczorek, A., Werther, P., Euchner, J. & Wombacher, R. Green- to far-red-emitting fluorogenic tetrazine probes – synthetic access and no-wash protein imaging inside living cells. *Chemical Science* **8**, 1506–1510 (2017).

50. Yang, J., Liang, Y., Šečkutė, J., Houk, K. N. & Devaraj, N. K. Synthesis and Reactivity Comparisons of 1-Methyl-3-Substituted Cyclopropene Mini-tags for Tetrazine Bioorthogonal Reactions. *Chemistry – A European Journal* **20**, 3365–3375 (2014).

51. Devaraj, N. K., Hilderbrand, S., Upadhyay, R., Mazitschek, R. & Weissleder, R. Bioorthogonal Turn-On Probes for Imaging Small Molecules inside Living Cells. *Angewandte Chemie International Edition* **49**, 2869–2872 (2010).

52. Carlson, J. C. T., Meimetis, L. G., Hilderbrand, S. A. & Weissleder, R. BODIPY–Tetrazine Derivatives as Superbright Bioorthogonal Turn-on Probes. *Angewandte Chemie International Edition* **52**, 6917–6920 (2013).

53. Karver, M. R., Weissleder, R. & Hilderbrand, S. A. Synthesis and Evaluation of a Series of 1,2,4,5-Tetrazines for Bioorthogonal Conjugation. *Bioconjugate Chemistry* **22**, 2263–2270 (2011).

54. Simon, C. *et al.* EPR imaging of sinapyl alcohol and its application to the study of plant cell wall lignification. *Chemical Communications* **57**, 387–390 (2021).

55. Knall, A.-C., Hollauf, M. & Slugovc, C. Kinetic studies of inverse electron demand Diels–Alder reactions (iEDDA) of norbornenes and 3,6-dipyridin-2-yl-1,2,4,5-tetrazine. *Tetrahedron Letters* **55**, 4763–4766 (2014).

56. Chi, W. *et al.* A unified fluorescence quenching mechanism of tetrazine-based

fluorogenic dyes: energy transfer to a dark state. Materials Chemistry Frontiers 5, 7012–7021 (2021).

57. Shen, Z., Reznikoff, G., Dranoff, G. & Rock, K. L. Cloned dendritic cells can present exogenous antigens on both MHC class I and class II molecules. The Journal of Immunology 158, 2723–2730 (1997).

58. van Leeuwen, T. et al. Bioorthogonal protein labelling enables the study of antigen processing of citrullinated and carbamylated auto-antigens. RSC Chemical Biology 2, 855–862 (2021).

59. Grimm, J. B. & Lavis, L. D. Caveat fluorophore: an insiders' guide to small-molecule fluorescent labels. Nature Methods 19, 149–158 (2022).

60. Hapuarachchige, S. et al. Design and synthesis of a new class of membrane-permeable triazaborolopyridinium fluorescent probes. Journal of the American Chemical Society 133, 6780–6790 (2011).

61. Grevengoed, T. J., Klett, E. L. & Coleman, R. A. Acyl-CoA metabolism and partitioning. Annual review of nutrition 34, 1–30 (2014).

62. Casares, D., Escribá, P. V & Rosselló, C. A. Membrane Lipid Composition: Effect on Membrane and Organelle Structure, Function and Compartmentalization and Therapeutic Avenues. International Journal of Molecular Sciences vol. 20 2167 Preprint at (2019).

63. Moessinger, C. et al. Two different pathways of phosphatidylcholine synthesis, the Kennedy Pathway and the Lands Cycle, differentially regulate cellular triacylglycerol storage. BMC Cell Biology 15, 43 (2014).

64. Smeenk, M. L. W. J., Agramunt, J. & Bonger, K. M. Recent developments in bioorthogonal chemistry and the orthogonality within. Curr Opin Chem Biol 60, 79–88 (2021).

65. Chehrehasa, F., Meedeniya, A. C. B., Dwyer, P., Abrahamsen, G. & Mackay-Sim, A. EdU, a new thymidine analogue for labelling proliferating cells in the nervous system. Journal of Neuroscience Methods 177, 122–130 (2009).

66. Peláez, R., Pariente, A., Pérez-Sala, Á. & Larráyoz, I. M. Sterculic Acid: The Mechanisms of Action beyond Stearoyl-CoA Desaturase Inhibition and Therapeutic Opportunities in Human Diseases. Cells vol. 9 140 Preprint at (2020).

67. van Onzen, A. H. A. M. et al. Bioorthogonal Tetrazine Carbamate Cleavage by Highly Reactive trans-Cyclooctene. Journal of the American Chemical Society 142, 10955–10963 (2020).